Control strategy on two-/four-electron pathway of water splitting by multi-doped carbon based catalysts

Xiuqin Wu,[§a] *Cheng Zhu,*[§a] *Liping Wang,*[a] *Sijie Guo,*[a] *Yalin Zhang,*[a] *Hao Li,*[a] *Hui Huang,**[a] *Yang Liu,**[a] *Junwang Tang,**[b] *and Zhenhui Kang**[a]

[a.]Jiangsu Key Laboratory for Carbon Based Functional Materials & Devices, Institute of Functional Nano & Soft Materials (FUNSOM), Soochow University, 199 Ren'ai Road, Suzhou, 215123, Jiangsu, PR China E-mail: hhuang0618@suda.edu.cn (H. Huang); yangl@suda.edu.cn (Y. Liu); zhkang@suda.edu.cn (Z.H. Kang).

[b.]Department of Chemical Engineering, University College London, London, United Kingdom. Email: junwang.tang@ucl.ac.uk (J.W. Tang).

[§]These authors contributed equally to this work.

ABSTRACT

Overall photocatalytic water splitting can proceed through a four-electron or two-electron/two-step pathway. However, it is challenging to manipulate the two- or four-electron pathway. Here, we present that a nitrogen, sulfur, transition metal-codoped carbon based nanostructure, which exhibits reliable photocatalytic ability and satisfactory photostability in water splitting without a need of sacrificial agents. Note that in present system, the transition metal doped structure (M =

Cr, Cd, Fe, Zn) as a photocatalyst splits water into H_2 and O_2 through a two-electron pathway while rare earth (Re) elements (M = Re = Sm, Ce, Eu, Pr, Er) doped one as photocatalysts via a four-electron pathway and carbon dots herein work as an electron acceptor and a reduction cocatalyst.

KEYWORDS: carbon based catalysts, photocatalyst, overall photocatalytic water splitting, two-electron pathway, four-electron pathway

INTRODUCTION

Harvesting solar energy for the production of hydrogen from water is an ultimate clean and renewable energy strategy for the global environmental issues and the energy crisis.[1-4] The design and fabrication of high-efficiency, stable and low-cost photocatalysts are key issues for the water splitting. In general, water splitting is an endothermic process, which demands the energy that equal or greater than enthalpy change (ΔH) required for the decomposition of water into hydrogen and oxygen.[5-7] Overall water splitting, which directly decompose water into H_2 and O_2, is an ultimate method for production of H_2. However, even intense efforts have been devoted to the design and fabrication of photocatalysis for overall water splitting, big challenges are still remained: (i) few complete photocatalytic water splitting systems are explored compared to photocatalysts for hydrogen production with sacrificial agents and cocatalysts; (ii) few currently reported photocatalysts show considerable stability; (iii) a large overpotential for

overall four-electron water oxidation to O_2 needs to be overcome; and (iv) H_2O_2 (produce by competing two-electron reaction) often poisons the photocatalysts.[3,8-12]

The photocatalytic overall water splitting can proceed through four-electron pathway ($H_2O \rightarrow H_2+O_2$) and two-electron two-step pathway ($H_2O \rightarrow H_2+H_2O_2$; $H_2O_2 \rightarrow H_2O+O_2$).[3] The four-electron process for oxygen evolution (1.23 eV *vs.* SHE) is a more workable strategy than the two-electron process for H_2O_2 formation (1.78 eV *vs.* SHE) from the point of view of thermodynamics. The second step of the two-electron two-step pathway ($H_2O_2 \rightarrow H_2O+O_2$) is however exothermic (ΔG = -106.1 kJ/mol),[13,14] and if H_2O_2 has no significant negative influence on the activity of catalysts and the generated H_2O_2 could be disintegrated quickly by the catalysts, the two-electron two-step pathway may also provide a viable and effective approach toward overall water splitting into H_2 and O_2. Nevertheless, it is difficult to control the four-electron or two-electron pathway in the process of H_2 and O_2 evolution from water splitting.

Carbon dots (CDs) exhibit superiority of low cost, easy fabrication, earth-abundance, rapid electron transfer, and electron reservoir properties.[15-17] CDs not only can be regarded as excellent catalysts,[18,19] but also used as functional components for photocatalysts and electrocatalysts.[20-25] At the same time, the multicomponent nanostructure may further improve the catalytic performance.[26-30] It is reported that the codoping of sulphur (S) and nitrogen (N) with additional electrons can enhance the photo-response property, generate higher electroconductivity, and facilitate transport of the photo induced charge carriers to the surfaces of the catalysts, hence reduce the recombination of the electron-hole pairs.[31-35] On the other hand, phthalocyanine (Pc)-

like compounds are an intensely aromatic macrocyclic structure, which have long been examined as catalysts for redox reactions.[36,37] Motivated by the photoelectric and catalytic activities of Pc, we further expect to combine Pc species with CDs as a way to design and construct carbon based photocatalysts for overall water splitting.

Herein, we present nitrogen, sulfur, transition metal elements-codoped carbon nanostructures prepared by a pyrolysis method. The products are carbon nanostructure based on CDs and Pc structures, namely, what we call "multi- doped carbon based nanostructure" [$(SMPc)_n$/CDs]. Note that, here, transition metal coordination structure is denoted as [$(SMPc)_n$/CDs, M = Cr, Cd, Fe, Zn] and nitrogen, sulfur, rare earth (Re) elements-codoped carbon based nanostructure [rare earth oxide compounds structure as [$(SMPc)_n$/CDs, M = Re = Sm, Ce, Eu, Pr, Er]]. As photocatalysts, they exhibit efficient photocatalytic ability and good photostability for overall water splitting without sacrificial agents. In present system, the $(SMPc)_n$/CDs (M = Cr, Cd, Fe, Zn) composite splits water into H_2 and O_2 through a two-electron pathway, while overall photocatalytic water splitting over $(SMPc)_n$/CDs (M = Re = Sm, Ce, Eu, Pr, Er) photocatalysts is a four-electron pathway. Moreover, CDs herein work as an electron acceptor and a reduction cocatalyst.

EXPERIMENTAL SECTION

Materials

Urea, samarium chloride hexahydrate ($SmCl_3 \cdot 6H_2O$), cerium chloride heptahydrate ($CeCl_3 \cdot 7H_2O$), erbium chloride hexahydrate ($ErCl_3 \cdot 6H_2O$), praseodymium chloride hexahydrate ($PrCl_3 \cdot 6H_2O$), europium chloride hexahydrate ($EuCl_3 \cdot 6H_2O$), chromic chloride hexahydrate ($CrCl_3 \cdot 6H_2O$), cadmium chloride hydrate ($CdCl_2 \cdot 2.5H_2O$), ferric chloride hexahydrate ($FeCl_3 \cdot 6H_2O$), zinc chloride ($ZnCl_2$), ammonium molybdate tetrahydrate [$(NH_4)_2MoO_4 \cdot 4H_2O$], pyromellitic dianhydride (PMDA), 4-sulphophthalic anhydride, silver nitrate ($AgNO_3$), lead nitrate [$Pb(NO_3)_2$], 1-butyl-3-methylimidazolium hexafluorophosphate (BMIMPF6), and ferrocene are of analytic purity and used without further purification.

Synthesis of CDs and $(SMPc)_n$/CDs

CDs were synthesized by an electrochemical etching method with graphite rods as carbon source reported by our group previously.[38] The obtained brown CDs solution with a uniform size in range of 5-10 nm is frozen drying to get the fluffy CDs powder. After that, 50 mg CDs powder was added in 100 mL ultrapure water to form a solution of 0.5 g/L. $(SMPc)_n$/CDs was fabricated by a modified method reported by Frank and co-workers previously.[39] Briefly, 18 mmol (1.13 g) urea, 1.9 mmol metal chloride, 0.28 mmol (0.063 g) PMDA, and 0.02 g $(NH_4)_2MoO_4 \cdot 4H_2O$ were added to a crucible and mixed well. Then the mixture was heated to molten state by an alcohol burner. Afterwards, 0.5 g 4-sulfophthalic anhydride was quickly put into the crucible under vigorous stirring until the mixture appeared dramatic expansion. Subsequently, 4 mL CDs were injected dropwise into the crucible. At last, the mixture was maintained at 250 °C for 90 min in

muffle furnace. Finally, a fluffy solid was obtained, and it was thoroughly washed with diluted hydrochloric acid and distilled water several times to remove solid oxides that may form and other impurities. Then, the obtained samples were dried in a vacuum oven at 60 °C for 12 h. The $(SMPc)_n$ was synthesized under the same conditions without CDs. Under the real condition of the reaction, the prepared $(SMPc)_n$ (M = Cr, Cd, Fe, Zn) was a transition metal coordination structure,[40] and the $(SMPc)_n$ (M = Sm, Ce, Eu, Pr, Er) was a complex of metal-free phthalocyanine and rare earth oxide.[41,42]

Photocatalytic activity test

The photocatalytic reactions were conducted in a Pyrex glass photoreactor with a flat window at the top for illumination connected to a closed gas-circulation system. 80 mg catalyst powder was dispersed in 100 mL ultrapure water, and then the system was completely degassed to remove air through a vacuuming procedure. Under ambient conditions and constant stirring, the suspension was irradiated by AM 1.5G solar simulator (MICROSOLAR 300, Beijing Perfectlight Co. Ltd, China). For evolved gas detection, an online GC-7900 gas chromatograph set up with a thermal conductivity detector (TCD) and 5 Å molecular sieve columns was employed. The oven, injection port and detector temperatures of gas chromatograph were held at 80, 100, and 120 °C, respectively. Argon (Ar) was used as carrier gas with the flow rate of 30 mL/min. To check the reproducibility and stability of catalysts, the suspension after reaction was centrifuged and reused for repeated tests.

Determination of reduction sites and oxidation sites

It has been reported that Ag particles are reductively photodeposited on reduction sites and PbO_2 particles are oxidatively photodeposited on oxidation sites as follows:[43,44]

$$Ag^+ + e^- \rightarrow Ag$$

$$Pb^{2+} + 2H_2O + 2h^+ \rightarrow PbO_2 + 4H^+$$

Therefore, in our work, 2 mg catalyst powder was dispersed in 30 mL of ultrapure water, then the suspension was irradiated by a 300 W Xe-lamp for 3 h under continuous stirring. Subsequently, about 0.5 mg $AgNO_3$ [or $Pb(NO_3)_2$] powder was added to the above suspension and the mixture was continuously stirred for 30 min in darkness. The obtained intermixture was centrifuged and further analysed by high-resolution transmission electron microscopy (HRTEM) measurements to determine the reduction sites (or oxidation sites).

Characterizations

Scanning electron microscopy (SEM) and energy dispersive X-ray spectroscopy (EDS) measurements were carried out using a FEI-quanta 200 scanning electron microscope with an accelerating voltage of 20 kV. Transmission electron microscopy (TEM) and High-resolution TEM (HRTEM) images were taken on a FEI-Tecnai F20 transmission electron microscope with an accelerating voltage of 200 kV. The TEM samples were prepared through dropping the solution onto a copper grid with polyvinyl supporting film and dried in air. The X-ray diffraction spectra (XRD) measurements were performed on an X-ray diffractometer (Empyrean, Holland

Panalytical) with nickel-filtered Cu Kα (λ = 0.154178 nm) radiation as the X-ray source. Fourier transform infrared spectra (FTIR) were obtained with a Nicolet 6700 spectrometer using a standard KBr pellet technique in the scan range of 400-4000 cm^{-1}. X-ray photoelectron spectra (XPS) were carried out using a KRATOS Axis ultra-DLD X-ray photoelectron spectrometer with a monochromatised Mg Kα X-ray source (hv = 1283.3 eV). The UV-vis spectra were obtained via a Lambda 750 (Perkin Elmer) spectrophotometer in the wavelength range of 200-800 nm.

Electrochemical Characterization

The cyclic voltammetry (CV), linear sweep voltammograms (LSV), current-time (i-t) curves and electron transfer number (n) experiments were carried out in a standard three-electrode cell with a computer-controlled CHI 920C workstation (CH Instruments, Chenhua, Shanghai, China) at room temperature. A platinum (Pt) wire and an Ag/AgCl (3 M KCl) electrode or a saturated calomel electrode (SCE) were used as the counter electrode and the reference electrode, respectively. The glassy carbon (GC) electrode (3 mm diameter) was polished to a mirror finish, thoroughly cleaned and dried before use. 10 μL catalyst solution (1.5 $mg \cdot mL^{-1}$) and 5 μL 0.5 wt % Nafion solution were dropped onto the surface of a treated GC electrode and left to dry naturally to prepare the working electrode. Before electrochemical testing, the working electrode was immersed into the electrolyte and activated for 30 min to keep it stable. The CV curves were performed in N_2-saturated 0.1 M BMIMPF6 solution with a scan rate of 50 mV/s. The i-t curves were gained at open circuit potential in ultrapure water. The

electron transfer number was studied by rotating disk-ring electrodes (RRDE). The RRDE collection experiments for $(SMPc)_n$/CDs were performed in N_2 saturated ultrapure water at 100 mV/s with a rotation speed of 1600 rpm. The disk potential was set at open circuit potential. The ring potential was set at 0.9 V *vs.* SCE. A Xe lamp (300 W) positioned 2 cm away from the working electrode was used as the light source.

Results and discussion

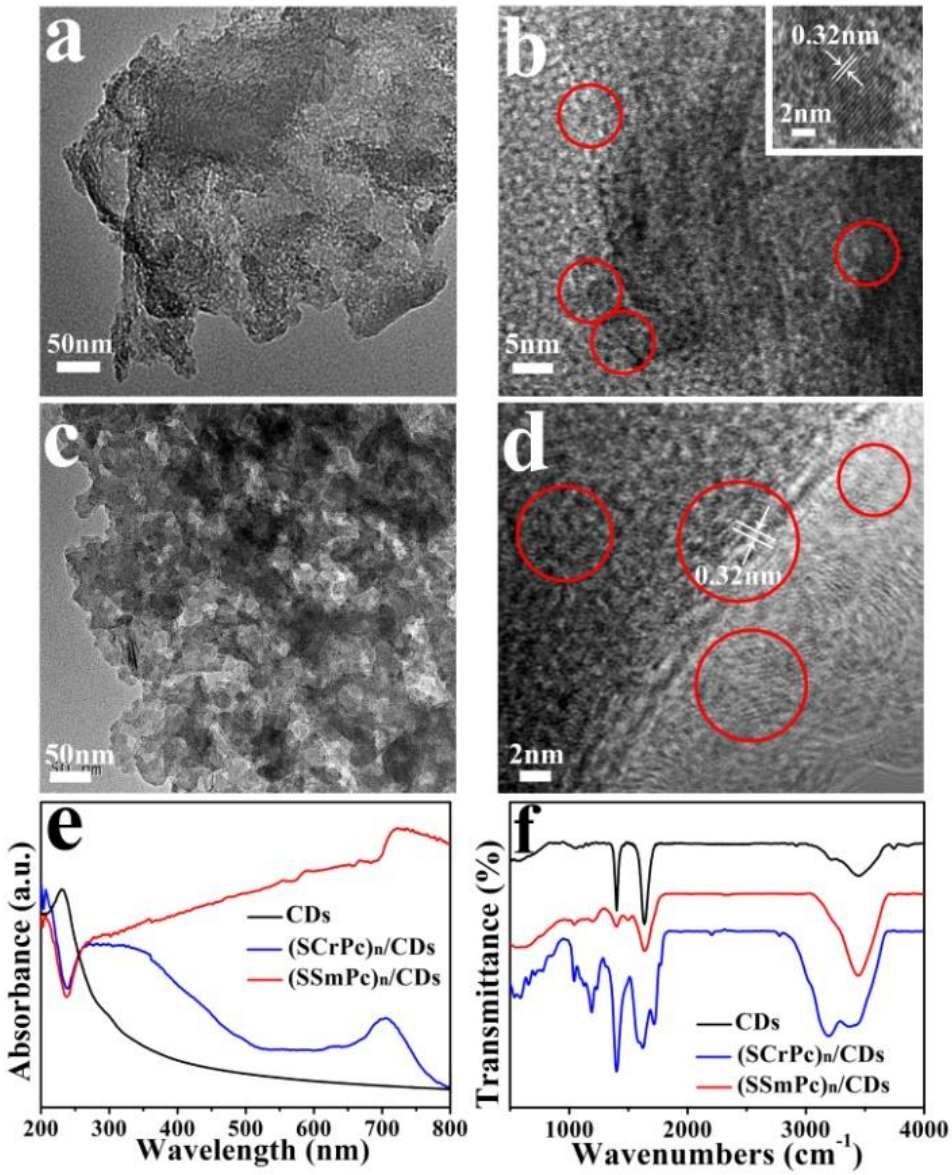

Figure 1. Typical TEM (a) and HRTEM (b) images of $(SCrPc)_n$/CDs, the scale bar inserted in (b) is 2 nm. Typical TEM (c) and HRTEM (d) images of $(SSmPc)_n$/CDs. UV-vis absorption spectra (e) and FTIR spectra (f) of $(SSmPc)_n$/CDs (red trace), $(SCrPc)_n$/CDs (blue trace) and CDs (black trace), respectively. The red circles in Figure b and d represent CDs.

In our experiments, briefly, a modified method of solid-state synthesis of Pc was used and CDs as a reaction agent were introduced.[39,45] Then the obtained products are the so called "multi-doped carbon nanostructure" [$(SMPc)_n$/CDs]. Figure 1a shows TEM images of $(SCrPc)_n$/CDs, indicating the obtained nanostructure is irregular. Figure S2 displays the TEM and HRTEM images of the as-prepared CDs, from which we can see that these CDs possess uniform size in the range of 5-10 nm and the clear lattice spacing of 0.32 nm is in good agreement with the (002) crystallographic plane of graphite.[38] Figure 2b exhibits the HRTEM image of $(SCrPc)_n$/CDs. As shown, the CDs are consistently deposited on the carbon nanostructure and as stable cocatalysts, in which the lattice fringes of (002) plane of graphitic carbon with an interplanar spacing of 0.32 nm could be easily identified.[46] Figure S3 describes the SEM image, as well as the corresponding EDS elemental mapping images of $(SCrPc)_n$/CDs, which declare that the C, N, O, S, and Cr were uniformly distributed in the carbon nanostructure and C, N, O, S and Cr were successfully doped in the nanostructure. From the TEM image of $(SSmPc)_n$/CDs (Figure 1c), it can be observed that the $(SSmPc)_n$/CDs were also morphologically irregular and CDs were spotted on the surface of the carbon nanostructure. To visualize the spatial distribution of elements, the EDX technique was used to analyze the $(SSmPc)_n$/CDs, and the results are shown in Figure S4. It can be seen that the elements of C, N, O, S and Sm spread evenly on the whole carbon nanostructure. The HRTEM image of $(SSmPc)_n$/CDs is shown in Figure 1d with an interplanar spacing of 0.32 nm, assigning to the (002) plane of graphitic carbon. These results confirmed that the CDs were successfully loaded onto the obtained carbon nanostructures.

The optical properties of the as-prepared samples were investigated by UV-vis absorption spectra (Figure 1e). It can be clearly observed that both $(SCrPc)_n$/CDs (blue trace) and $(SSmPc)_n$/CDs (red trace) possess stronger and wider visible light absorption bands compared with CDs (black trace), which only have absorption peak from 230-280 nm ascribed to various π-π* and n-π* transitions.[47] Moreover, the enhanced light absorption is helpful for improving the capacity of photocatalytic overall water splitting. Fourier transform infrared (FTIR) spectra were employed to characterize the surface functional groups of $(SMPc)_n$/CDs. As shown in Figure 1f, the FTIR spectrum of CDs (black trace) demonstrates CDs prepared in our work possess ample functional groups. The peak around 1630 cm^{-1} corresponds to the stretching vibrations of C=C/C=O bonds.[48,49] The absorption bands at 3400 cm^{-1} and 1050 cm^{-1} are assigned to C-OH and C-O-C, respectively, which confirms the existence of carboxyl groups (-COOH).[49] For $(SCrPc)_n$/CDs (blue trace) and $(SCrPc)_n$/CDs (red trace), both the characteristic peaks of CDs were also observed, indicating the existence of CDs in the complex photocatalysts. The bands in the region of 1640-1630 cm^{-1} arise from the stretching vibrations of C=N bonds,[48] while the weak peaks at 1200-1600 cm^{-1} region correspond to the characteristic absorption of the typical aromatic CN heterocycles.[50] The crystalline structure of the as-prepared samples have been further confirmed by XRD (Figure S5 and S6). The XRD pattern of CDs shows a prominent peak at 26° referring to the amorphous carbon[38,51]. In the XRD patterns of $(SMPc)_n$/CDs, the broad peaks at about 27° correspond to amorphous carbon, and no extra characteristic peaks were detected. These results indicate that the as-prepared $(SMPc)_n$/CDs are amorphous carbon structure.

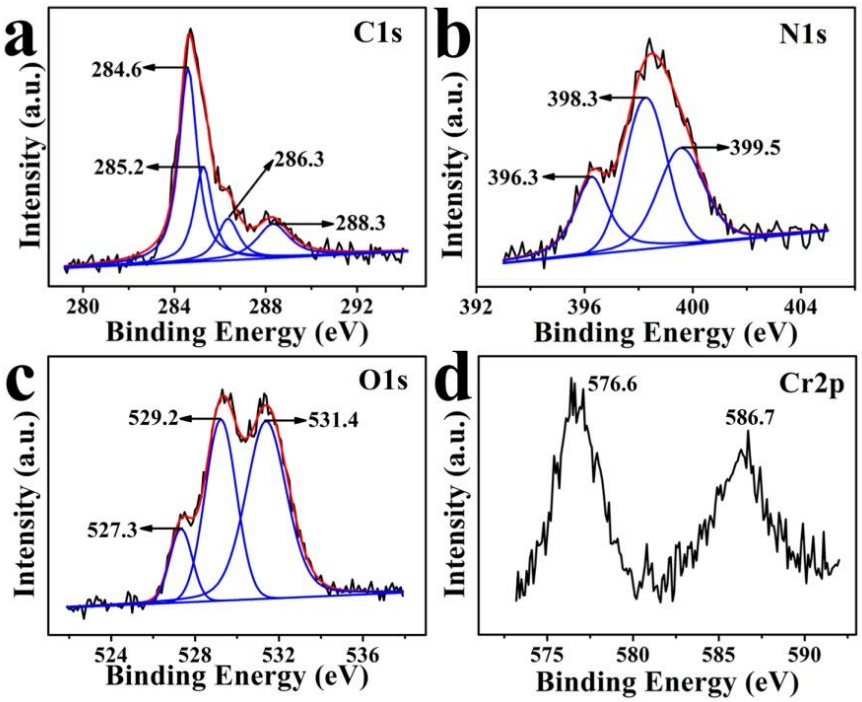

Figure 2. The high resolution C 1s (a), N 1s (b), O 1s (c) and Cr 2p (d) XPS spectra of $(SCrPc)_n$/CDs.

The X-ray photoelectron spectroscopy (XPS) was performed to further explore the surface compositions and chemical states of $(SMPc)_n$/CDs, and the corresponding results are shown in Figure 2, Figure 3 and Figure S7. Figure S7a shows the fully scanned spectrum of $(SCrPc)_n$/CDs, which confirms the existence of C, N, O, S and Cr elements (the signal of In is due to the substrate). The high resolution C 1s XPS spectra of $(SCrPc)_n$/CDs (Figure 2a) could be divided into four deconvoluted peaks with binding energies of 284.6, 285.2, 286.3 and 288.3 eV, which correspond to C-C/C=C, (C)3-N/C-OH and N-C=N/C=O, respectively.[3,52] The N 1s core level spectrum of $(SCrPc)_n$/CDs (Figure 2b) can be fitted into three peaks, which can be ascribed to N-Cr (396.3 eV), C=N-C (398.3 eV), and N-(C)3 (399.5 eV), respectively.[3,53] The presence of

N-Cr may demonstrate the formation of transition metal coordination structure (metal phthalocyanine). The O1s core level spectrum presented in Figure 2c is fitted with three different signals with binding energies of 527.3, 529.2, and 531.4 eV, which are attributed to O-H, O-Cr and adsorbed water, respectively.[49] The high resolution Cr 2p spectrum of $(SCrPc)_n$/CDs shown in Figure 2e suggested Cr 2p 1/2 and Cr 2p 3/2 peaks located at 586.7 and 576.6 eV, respectively, which can be assigned to chromic oxide.[54,55] In Figure S7b, the full XPS survey spectrum of $(SSmPc)_n$/CDs shows the C 1s, N 1s, O 1s, S 2p and Sm 3d peaks. The high resolution C 1s XPS spectrum of $(SSmPc)_n$/CDs is shown in Figure 3a, which represent four main peaks located at about 284.6, 285.5, 286.4 and 288.8 eV, corresponding to C-C sp^2 and sp^3 hybridized components, C-N/C-OH and N-C=N/C=O, respectively.[56,57] Deconvolution of the high-resolution N 1s XPS spectra of $(SSmPc)_n$/CDs in Figure 3b indicates three prominent peaks at 398.7, 399.9 and 401.1eV, attributed to C-N-C, pyridine and urotropine-type nitrogen, respectively.[50,58] The three peaks that can be distinguished in the XPS O 1s spectrum of $(SSmPc)_n$/CDs are shown in Figure 3c. The three resolved peaks of O 1s core level spectrum at about 530.2, 531.8 and 533.7 eV are assigned to lattice oxygen, surface hydroxyl groups, and adsorbed water, respectively.[59] The high resolution Sm 3d spectrum of $(SSmPc)_n$/CDs (Figure 3d) shows two bands at binding energies of 1084.5 and 1111.5 eV, which are attributed to the 3d 5/2 and 3d 3/2 ionization of Sm^{3+}, respectively, indicating that Sm species may be existed in the form of Sm_2O_3.[60] These results demonstrate that the structure of $(SCrPc)_n$/CDs is different from that of the $(SSmPc)_n$/CDs (as illustrated in Figure S8).

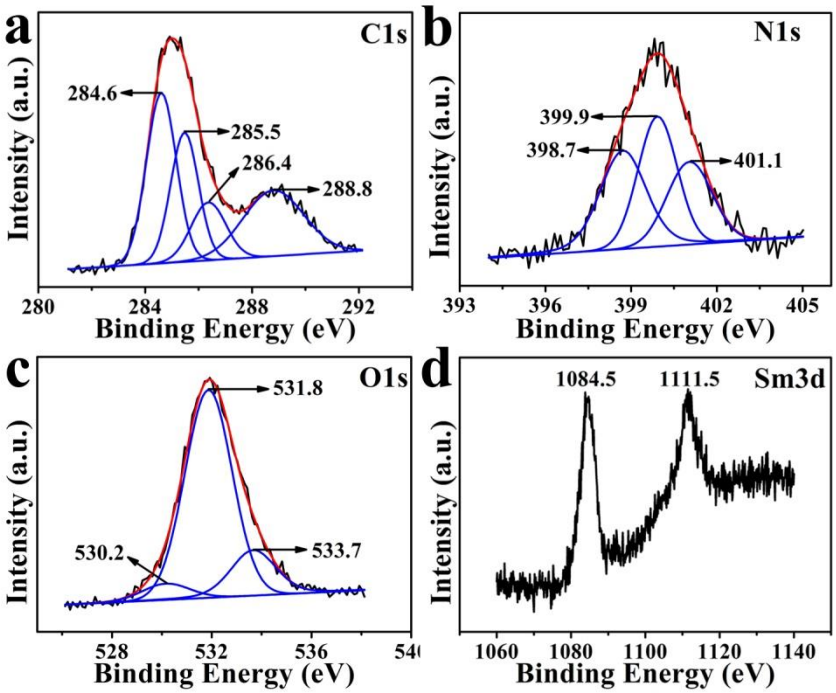

Figure 3. The high resolution C 1s (a), N 1s (b), O 1s and (c) Sm 3d, (d) XPS spectra of $(SSmPc)_n$/CDs.

To evaluate the highest occupied molecular orbital (HOMO) and the lowest unoccupied molecular orbital (LUMO) of $(SMPc)_n$/CDs, the cyclic voltammetry (CV) experiments were performed. Figure 4a and 4c display the cyclic voltammograms (CV) of $(SCrPc)_n$/CDs and $(SSmPc)_n$/ CDs (the ferrocene redox system was introduced as an external standard). The HOMO and LUMO energy levels were calculated from the onset of oxidation (E_{ox}) and reduction (E_{red}) potentials as determined by CV and the reference energy level for ferrocene (4.8 eV below the vacuum level) according to the following equations:[61]

$$E_{HOMO} = - (E_{onset}^{ox} - E_{ferrocene} + 4.80)\ eV$$

$$E_{LUMO} = - (E_{onset}^{red} - E_{ferrocene} + 4.80)\ eV$$

$$E_g \text{ (band gap)} = E_{onset}^{ox} - E_{onset}^{red}$$

Where $E_{ferrocene}$ is the onset of the oxidation potential (*vs.* Ag/AgCl) of ferrocene. The calculated HOMO/LUMO energy levels are -6.45/-4.04 eV for $(SCrPc)_n$/CDs, and -5.88/-3.89 eV for $(SCrPc)_n$/CDs. The calculated HOMO/LUMO energy levels and E_g values of different metal doped in $(SMPc)_n$/CDs photocatalysts are also shown in Table 1. Figure 4b shows band structure diagram of $(SCrPc)_n$/CDs, in which the conduction band (CB) and valence band (VB) of the photocatalyst straddled the reduction and oxidation potentials of water with +0 and +1.78 V (and +1.23 V) *vs.* reversible hydrogen electrode (RHE), respectively, thus photocatalytic water splitting into H_2 and O_2/H_2O_2 using $(SCrPc)_n$/CDs as a photocatalyst can be achieved in theory.[3] Figure 4d displays the energy level diagram of the $(SSmPc)_n$/CDs photocatalyst as compared to the potentials for water reduction and oxidation. As can be seen, the CB and VB of $(SSmPc)_n$/CDs have suitable potential levels for water reduction and oxidation. Therefore, the overall charge transfers are allowed in the present photocatalytic system.[27,62]

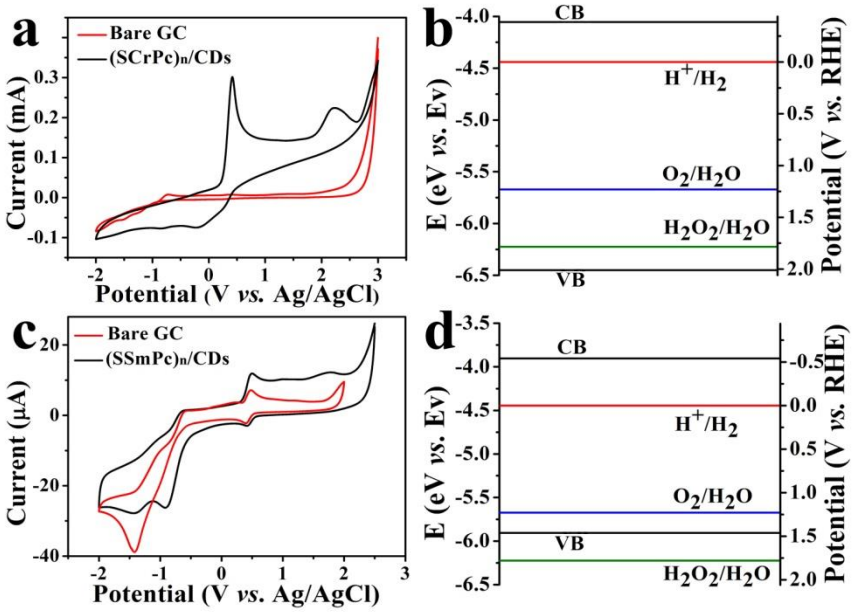

Figure 4. The CV (a) and band structure diagram (b) of $(SCrPc)_n$/CDs. The CV (c) and band structure diagram (d) of $(SSmPc)_n$/CDs.

Figure S9 shows the photoelectrical responses (instantaneous change in current upon illumination) of $(SCrPc)_n$/CDs (Figure S9a) and $(SSmPc)_n$/CDs (Figure S9b) under intermittent irradiation. Obviously, as shown in Figure S9a, the photocurrent density of the $(SCrPc)_n$/CDs rapidly increased to a value of 270.6 nA/cm^2 at the time of 30 s during illumination "On", and then sharply returned to its initial value when the light was turned "Off". The ''On'' and ''Off''-state currents for each cycle shown here were maintained within the noise level, further demonstrating excellent stability and reproducible characteristics of the photocurrent for $(SCrPc)_n$/CDs photocatalyst over this time interval. From Figure S9b, the $(SSmPc)_n$/CDs sample exhibits a residual current photocurrent when light immediately removed. The relatively slower decay of the photocurrent may be due to trapped charge carriers with a prolonged lifetime. These

results suggested that the $(SMPc)_n$/CDs catalysts are of high photoelectric response and good photocurrent stability.

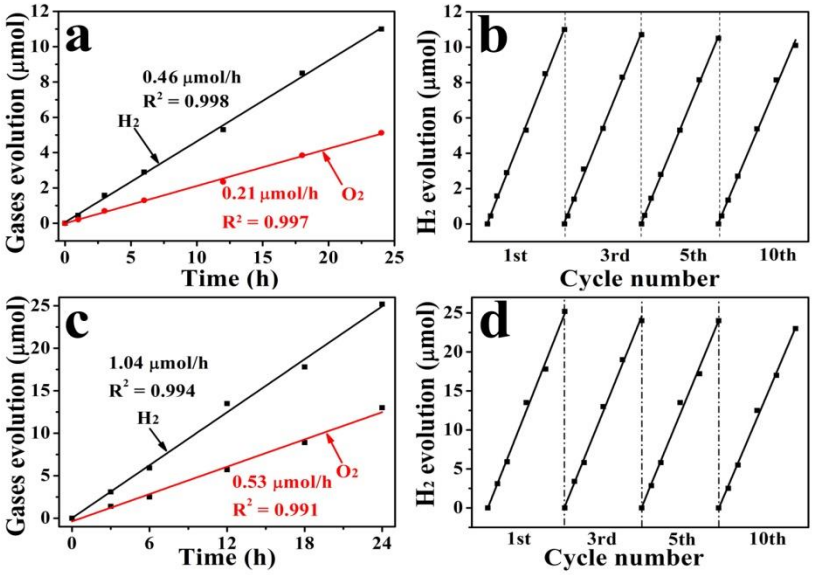

Figure 5. (a) Typical time course of H_2 and O_2 production, and (b) the stability of photocatalytic water splitting over $(SCrPc)_n$/CDs photocatalyst. (c) Typical time course of H_2 and O_2 production, and (d) the stability of photocatalytic water splitting over $(SSmPc)_n$/CDs photocatalyst.

In the following experiments, the performance of photocatalytic water splitting under sunlight irradiation using $(SMPc)_n$/CDs carbon nanostructures as photocatalysts was investigated without any sacrificial agent or cocatalyst. Figure 5a describes the photocatalytic activity of $(SCrPc)_n$/CDs for water splitting. The H_2 and O_2 in a molar ratio of H_2/O_2 is 2.17 were detected by gas chromatograph in the experimental period. The H_2 and O_2 evolution rates (0.46 μmol/h and 0.21 μmol/h, respectively) remained almost unchanged for 24 h on course. For the

$(SSmPc)_n$/CDs as photocatalyst (Figure 5c), both H_2 and O_2 are produced simultaneously with a H_2/O_2 ratio close to 2.0 (H_2 evolution rate of 1.04 μmol/h and O_2 evolution rate of 0.53 μmol/h). Table 1 presents photocatalytic activities of all the $(SMPc)_n$/CDs for water splitting. It can be seen that part of $(SMPc)_n$/CDs (M = Sm, Ce) have shown higher catalytic activity than that of $(SMPc)_n$/CDs (M = Cr, Cd, Fe, Zn), which may result from the orbital hybridization of 4f electrons that able to inhibit the combination of photo-excited electrons and holes and enlarge the light adsorption.[63] Good stability is one of the important factors for the practical applications of photocatalysts in overall water splitting. Figure 5b and d confirm stable photocatalytic activities of $(SCrPc)_n$/CDs and $(SSmPc)_n$/CDs as photocatalysts under optimum reaction conditions. After the first cycle (24 h), H_2 could still be collected with nine more cycles. The average H_2 gas evolution rates for $(SCrPc)_n$/CDs and $(SSmPc)_n$/CDs are 0.43 μmol/h and 1.01 μmol/h, respectively. The slight reduction of the H_2 evolution activity may probably attribute to the loss of photocatalysts in the filtration processes.

A series of control experiments were also performed. First, the control experiments were carried out under different conditions: (1) in the presence of $(SMPc)_n$/CDs but under dark and (2) with full range irradiation (UV + visible light) but in the absence of the $(SMPc)_n$/CDs. The results demonstrated that no H_2 was detected. Then, we further compared the photocatalytic abilities of $(SMPc)_n$/CDs with different atomic percent. In the preparation process of $(SMPc)_n$/CDs, we only adjusted the amount of urea and CDs with other conditions unchanged. Table S1 and S2 shows

the relationship between the rate of H_2 evolution and the volume of CDs (0, 4, 8 mL, the concentration of CDs was 0.5 g/L) over $(SMPc)_n$/CDs in the case of the mass of the urea was 0.56 g, 1.13 g and 1.69 g, respectively. It can be found that the $(SCrPc)_n$/CDs and $(SSmPc)_n$/CDs did not exhibit obvious performance of photocatalytic hydrogen production regardless of the amount of CDs when the mass of urea was 0.56 g or 1.69 g, which may be due to the fact that the $(SMPc)_n$ structure (Pc structure) did not form in the reaction process. On the other hand, even though the mass of urea was 1.13 g, the obtained $(SMPc)_n$/CDs carbon nanostructure as a photocatalyst have barely photocatalytic water splitting properties when the amount of CDs was 0 mL. With the increase of the volume of CDs (8 mL, the urea was 1.13 g), the photocatalytic activity of $(SMPc)_n$/CDs gradually decreased [0.27 μmol/h for $(SMPc)_n$/CDs, 0.86 μmol/h for $(SSmPc)_n$/CDs], owing to the fact that the excess CDs suppressed the formation of the $(SMPc)_n$/CDs carbon nanostructures. The maximum H_2 evolution was obtained when the injected CDs was 4 mL. These results indicate the CDs and $(SMPc)_n$ both play vital roles in overall water splitting. Significantly, the best overall water splitting was achieved under the conditions of using 1.13 g urea and 4 mL CDs simultaneously. It turned out that the N, S, and metal concentrations exhibit a synergistic effect on the photocatalytic activity of the $(SMPc)_n$/CDs system.

Table 1. Electrochemical data and photocatalytic activities of $(SMPc)_n$/CDs photocatalysts.

Photocatalysts	E_{HOMO} (eV)	E_{LUMO} (eV)	n	Rate (μmol/h)	
				H_2	O_2
$(SCrPc)_n$/CDs	**-6.45**	**-4.04**	**1.88**	**0.46**	**0.21**
$(SCdPc)_n$/CDs	-6.30	-4.06	1.84	0.40	0.19
$(SFePc)_n$/CDs	-6.41	-4.12	1.68	0.24	0.11
$(SZnPc)_n$/CDs	-6.38	-4.07	1.79	<0.1	trace
$(SSmPc)_n$/CDs	**-5.88**	**-3.89**	**3.43**	**1.04**	**0.53**
$(SCePc)_n$/CDs	-6.19	-3.81	3.28	0.66	0.32
$(SEuPc)_n$/CDs	-6.21	-4.09	3.38	0.28	0.13
$(SPrPc)_n$/CDs	-6.60	-3.96	3.26	<0.1	trace
$(SErPc)_n$/CDs	-6.43	-3.87	3.19	<0.1	trace

For the sake of understanding photocatalytic water splitting over $(SMPc)_n$/CDs via two-electron or four-electron pathway, the following experiments were carried out. Figure 6a and b show RRDE collection experiments for $(SCrPc)_n$/CDs and $(SSmPc)_n$/CDs, respectively. The electron transfer number (n) could be calculated by the following equation:[3]

$$n = 4I_{disk}/(I_{disk}+I_{ring}/N)$$

where I_{disk} is the disk current density, I_{ring} is the ring current density and N is the RRDE collection efficiency. N refers to the fraction of the H_2O_2 formed at the disk that was collected at the ring[64] and it was experimentally determined to be 0.24. The n was calculated to be 1.88 for $(SCrPc)_n$/CDs, and 3.43 for $(SSmPc)_n$/CDs. The n for $(SMPc)_n$/CDs is shown in Table 1. We can conclude that $(SMPc)_n$/CDs (M = Cr, Cd, Fe, Zn) photocatalysts split water into H_2 and O_2 through a two-electron pathway ($H_2O \rightarrow H_2+H_2O_2$; $H_2O_2 \rightarrow H_2O+O_2$). While the $(SMPc)_n$/CDs (M = Re = Sm, Ce, Eu, Pr, Er) for overall photocatalytic water splitting is a four-electron pathway

($H_2O \rightarrow O_2+H_2$). The reasons for this phenomenon are possibly position of the VB in the photocatalysts, rich oxygen vacancy (or oxygen vacancy clustering) and high oxygen storage-release capacity in $(SMPc)_n$/CDs (M = Re = Sm, Ce, Eu, Pr, Er) that favorable to the formation of O_2 on the catalyst surface.[60,65,66]

The i-t curves of as-prepared $(SMPc)_n$/CDs under dark and light, respectively, (Figure 6c and d) were carried out to further study the photocatalytic activity in the process of water splitting. It turned out that the photocatalytic activity of $(SMPc)_n$/CDs maintained at a high level and there was no apparent catalyst deactivation phenomenon. The curves of $(SMPc)_n$/CDs show periodical current oscillation that may result from the generation, adsorption, desorption, and diffusion of H_2, O_2 and H_2O_2 in the water.[3]

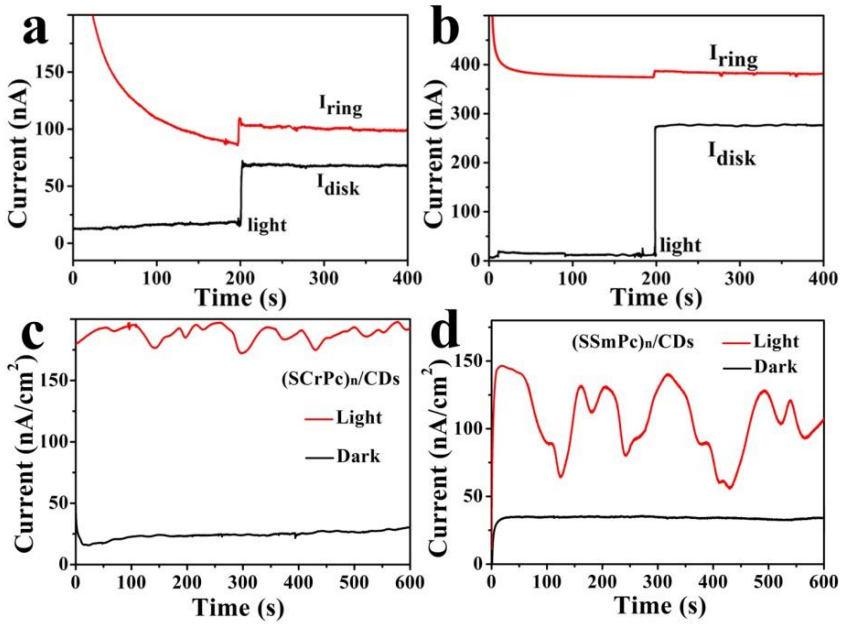

Figure 6. The RRDE collection experiments for $(SCrPc)_n$/CDs (a) and $(SSmPc)_n$/CDs (b). The i-t curve of $(SCrPc)_n$/CDs (c) and $(SSmPc)_n$/CDs (d) as photocatalysts.

Figure 7a and b show the UV-vis absorption spectra of free H_2O_2 in the reaction solution using $(SCrPc)_n$/CDs and $(SSmPc)_n$/CDs, which demonstrated that H_2O_2 was formed in the process of photocatalytic reaction over $(SCrPc)_n$/CDs, and no H_2O_2 was detected in the reaction solution after 24 h irradiation with $(SSmPc)_n$/CDs as catalysts (compared with Figure S1). These results are in agreement with measured band position (Figure 4b and d). The linear sweep voltammograms (LSV) curves for $(SMPc)_n$/CDs in different concentrations of H_2O_2 solution (Figure S10) exhibit that the $(SMPc)_n$/CDs catalysts have certain capability of decomposition of H_2O_2. Figure 7c and d shows O_2 evolution originates from H_2O_2 (5 mM, 100 mL) decomposition versus time curve using $(SMPc)_n$/CDs as catalysts under dark. As shown in Figure 7c, the O_2 evolution rate over $(SCrPc)_n$/CDs catalyst was about 24.2 μmol/h. Figure 7d shows O_2 evolution from H_2O_2 (5 mM) decomposition versus time curve using $(SSmPc)_n$/CDs catalysts, which demonstrated that the O_2 evolution rate over $(SCrPc)_n$/CDs photocatalyst was about 9.6 μmol/h (< 24.2 μmol/h). According to the acquired results, when using $(SCrPc)_n$/CDs for photocatalytic water splitting, the H_2O_2 in the reaction solution could be detected by UV-vis absorption spectra (Figure 7a and b, black trace). It can be inferred that the $(SCrPc)_n$/CDs photocatalysts can split water into H_2 and H_2O_2, and then the H_2O_2 can further decompose into O_2 and H_2O with the aid of the $(SCrPc)_n$/CDs catalysts. Moreover, the second step ($H_2O_2 \rightarrow H_2O+O_2$) is a rate-controlled

step, which claims the catalysts possess a strong catalytic ability for H_2O_2 decomposition (Figure 7c). Consequently, the $(SCrPc)_n$/CDs as a photocatalyst splits water into H_2 and O_2 through a two-electron two-step pathway ($H_2O \rightarrow H_2+H_2O_2$; $H_2O_2 \rightarrow H_2O+O_2$). For $(SSmPc)_n$/CDs, we assume that it also can split water into H_2 and H_2O_2 via a two-electron pathway. However, the H_2O_2 in the reaction solution cannot be detected based on UV-vis spectral data (Figure 7a and b, blue trace), which indicate either the generated H_2O_2 subsequently decomposed completely by the $(SSmPc)_n$/CDs catalysts or no H_2O_2 was produced. Taking into account results of band positions measured in Figure 4 and the number of electron transferred drawn from Figure 6, one can believe the latter is plausible. In other words, the $(SSmPc)_n$/CDs as photocatalysts should split water into H_2 and O_2 through a four-electron pathway ($H_2O \rightarrow H_2+O_2$).

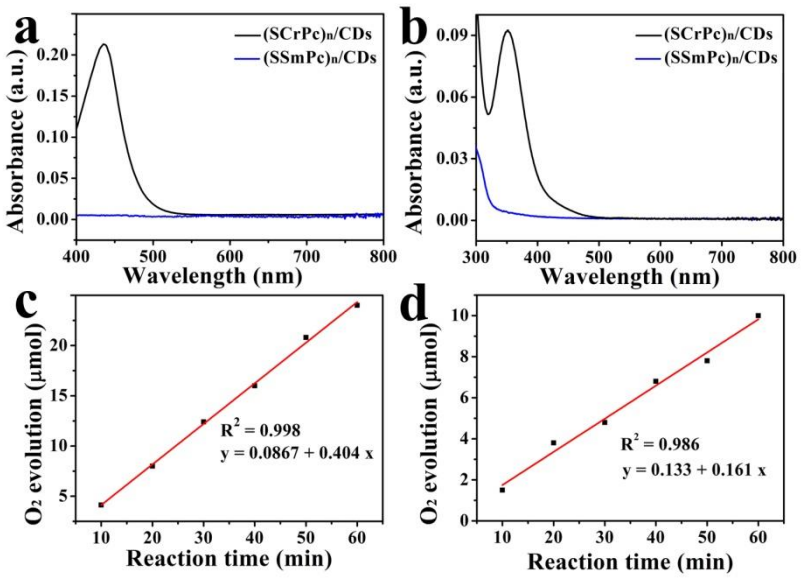

Figure 7. (a) UV-vis absorption spectra of free H_2O_2 in the reaction solution containing 1% *o*-tolidine over $(SCrPc)_n$/CDs (black trace) and $(SSmPc)_n$/CDs (blue trace) as photocatalysts. (b)

UV-vis absorption spectra of a reaction solution containing KI (excess) over $(SCrPc)_n$/CDs (black trace) and $(SSmPc)_n$/CDs (blue trace) as photocatalysts. The O_2 evolution from H_2O_2 (5 mM) decomposition versus time curve using $(SCrPc)_n$/CDs (c) and $(SSmPc)_n$/CDs (d) as catalysts under dark.

To further verify the roles of CDs in $(SMPc)_n$/CDs, the photo-induced electron transfer property of CDs was investigated. Figure S11 shows luminescence decays (485 nm excitation, monitored with 550 nm narrow band pass filter) of the CDs with (Figure S11a) 2, 4-dinitrotoluene and (Figure S11b) DEA, as well as corresponding Stern-Volmer plots (Figure S11c and d) for the quenching of luminescence quantum yields, in which Stern-Volmer quenching constants from linear regression was 30.4 and 25.4 M^{-1}, respectively. These data indicate that CDs possess electron donating and accepting capabilities. In the current catalyst system, CDs could act as electron acceptor. In the following experiments, $AgNO_3$ and $Pb(NO_3)_2$ as indicators were employed respectively to clarify the reduction and oxidation reaction sites in the $(SCrPc)_n$/CDs (Figure 8a and b) and $(SSmPc)_n$/CDs (Figure 8c and d) photocatalysts. As shown in Figure 8a and c, Ag particles were deposited on the surfaces of CDs in the carbon nanostructure, clear lattice spacings of 0.32 and 0.23 nm are in well agreement with the (002) crystallographic planes of graphitic carbon and (111) lattice planes of Ag,[67] respectively. It turned out that CDs should be active sites for H_2 evolution in the process of water splitting. The HRTEM image in Figure 8b shows interplanner spacing of 0.35 nm, which corresponds to the

(110) planes of PbO_2.[68] And clear lattice spacing of 0.28 nm in Figure 8d corresponds to the (111) planes of PbO_2.[69] It suggests the distribution of oxidation reaction sites on catalyst surface (away from CDs).

By combining all the analysis results, the main mechanisms were proposed towards the overall water splitting with $(SMPc)_n$/CDs as a photocatalyst, as shown in Figure S12. When $(SMPc)_n$/CDs was illuminated by light with its energy greater than the E_g of the photocatalyst, the photoexcited electrons and holes over the photocatalyst were quickly formed. After that, the transfer of the electrons to the surface of CDs and holes to the surface of $(SMPc)_n$/CDs carbon nanostructure rapidly occurs. Simultaneously, the photogenerated electrons reduce H^+, which is adsorbed on CDs surfaces, into H_2, and the holes are responsible for the oxidation from H_2O to H_2O_2 or O_2.[9,70] Then H_2O_2 was decomposed into O_2 and H_2O quickly. Additional studies devoted to increasing the rate of H_2 and O_2 production and the corresponding mechanisms are underway in our laboratory.

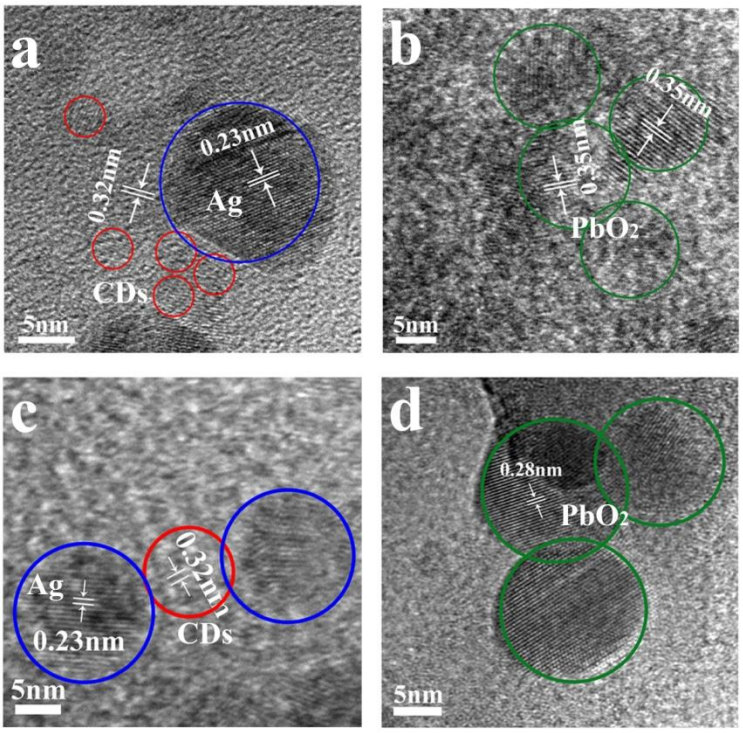

Figure 8. The HRTEM images of reduction sites (a) and oxidation sites (b) over $(SCrPc)_n$/CDs. The HRTEM images of reduction sites (c) and oxidation sites (d) over $(SSmPc)_n$/CDs. The red, blue and green circles represent CDs, Ag and PbO_2 particles, respectively.

CONCLUSIONS

We present that a nitrogen, sulfur, transition metal-codoped carbon based nanostructure [$(SMPc)_n$/CDs, M = Cr, Cd, Fe, Zn, Sm, Ce, Eu, Pr, Er] by a facile pyrolysis method exhibits efficient photocatalytic ability and photostability for overall water splitting without sacrificial agents. Among them, the CDs in $(SMPc)_n$/CDs nanostructure play important roles for photocatalytic water splitting, which not only improve charge seperation but more importantly provide active reduction reaction sites. Furthermore, overall photocatalytic water splitting has

been achieved on both photocatalysts but they have different reaction pathway. The $(SMPc)_n$/CDs (M = Cr, Cd, Fe, Zn) splits water into H_2 and O_2 through a two-electron pathway, while $(SMPc)_n$/CDs (M = Re = Sm, Ce, Eu, Pr, Er) photocatalyst is via a four-electron pathway. The current photocatalytic efficiency is not satisfactory, but can be improved by optimising the interface between a photocatalyst and CDs which is underway. In total, this discovery provides a regulatory method for the process of complete photocatalytic water splitting and a new possibility for the development of non-noble-metal photocatalytic systems for overall water splitting.

ASSOCIATED CONTENT

Supporting Information. This material is available free of charge via the Internet at http://pubs.acs.org.

AUTHOR INFORMATION

Corresponding Author

* E-mail: zhkang@suda.edu.cn (Z.H. Kang); yangl@suda.edu.cn (Y. Liu); hhuang0618@suda.edu.cn (H. Huang); junwang.tang@ucl.ac.uk (J.W. Tang).

Notes

The authors declare no competing financial interest.

ACKNOWLEDGEMENTS

This work is supported by the Collaborative Innovation Center of Suzhou Nano Science and Technology, the National Natural Science Foundation of China (51422207, 51132006, 51572179, 21471106, 21501126), the Specialized Research Fund for the Doctoral Program of Higher Education (20123201110018), the Natural Science Foundation of Jiangsu Province of China (BK20140310), China Postdoctoral Science Foundation (2014M560445, 2015T80581), and a project funded by the Priority Academic Program Development of Jiangsu Higher Education Institutions (PAPD).

REFERENCES

1. Xiang, Q.; Yu, J.; Jaroniec, M. *Chem. Soc. Rev.* **2012**, 41, 782-796.

2. Wang, W.; Tade, M; Shao, Z. *Chem. Soc. Rev.* **2014**, 44, 5371-5408.

3. Liu, J.; Liu, Y.; Liu, N.; Han, Y.; Zhang, X.; Huang, H.; Lifshitz, Y.; Lee, S.; Zhong, J.; Kang, Z. *Science* **2015**, 347, 6225, 970-974.

4. Bai, S.; Jiang, J.; Zhang, Q.; Xiong, Y. *Chem. Soc. Rev.* **2015**, 44, 2893-2939.

6. Chowdhury, P.; Malekshoar G.; Ray, M.; Zhu, J.; Ray. A. *Ind. Eng. Chem. Res.* **2013**, 52, 5023-5029.

7. Fabian, D.; Hu, S.; Singh, N.; Houle, F.; Hisatomi, T.; Domen, K.; Osterloh, F.; Ardo S. *Energy Environ. Sci.* **2015**, 8, 2825-2850.

8. Shen, S.; Shi, J.; Guo, P.; Guo, L. *Int. J. Nanotechnol.* **2011**, 8, 523-591.

9. Hisatomi, T.; Kubota, J.; Domen, K. *Chem. Soc. Rev.* **2014**, 43, 7520-7535.

10. Chen, X.; Shen, S.; Guo, L.; Mao, S. *Chem. Rev.* **2010**, 110, 6503-6570.

11. Esswein, A. J.; Nocera, D. G. *Chem. Rev.* **2007**, 107, 4022-4047.

12. Mateo, D.; Esteve-Adell, I.; Albero, J.; Royo, J. F. S.; Primo, A.; Garcia, H. *Nature communications* **2016**, 7, 11819-11819.

13. Choi, C.; Kwon, H.; Yook, S.; Shin, H.; Kim, H.; Choi, M. *J. Phys. Chem. C*. **2014**, 118, 30063-30070.

14. Kudo, A.; Miseki, Y. *Chem. Soc. Rev.* **2009**, 38, 253-278.

15. Li, H.; Kang, Z.; Liu, Y.; Lee, S. *J. Mater. Chem.* **2012**, 22, 24230-24253.

16. Tang, L.; Ji, R.; Cao, X.; Lin, J.; Jiang, H.; Li, X.; Teng, K.; Luk, C.; Zeng, S.; Hao, J.; Lau, S. *ACS Nano*, **2012**, 6, 5102-5110.

17. Li, H.; He, X.; Kang, Z.; Huang, H.; Liu, Y.; Liu, J.; Lian, S.; Tsang, C.; Yang, X. ; Lee, S. *Angew. Chem. Int. Ed.* **2010**, 49, 4430-4434.

18. Zhou, L.; Liu, J.; Zhang, X.; Liu, R.; Huang, H.; Liu, Y.; Kang, Z. *Nanoscale* **2014**, 6, 5831-5837.

19. Han, Y.; Huang, H.; Zhang, H.; Liu, Y.; Han, X.; Liu, R.; Li, H.; Kang. Z. *ACS Catal.* **2014**, 4, 781-787.

20. Zhang, H.; Huang, H.; Ming, H.; Li, H.; Zhang, L.; Liu, Y.; Kang, Z. *J. Mater. Chem*. **2012**, 22, 10501-10506.

21. Li, H.; Liu, R.; Liu, Y.; Huang, H.; Yu, H.; Ming, H.; Lian, S.; Lee, S.; Kang, Z. *J. Mater. Chem.* **2012**, 22, 17470-17475.

22. Tang, D.; Liu, J.; Wu, X.; Liu, R.; Han, X.; Han, Y.; Huang, H.; Liu, Y.; Kang, Z. *ACS Appl. Mater. Inter.* **2014**, 6, 7918-7925.

23. Yang, Y.; Liu, J.; Han, Y.; Huang, H.; Liu, N.; Liu, Y.; Kang, Z. *Phys. Chem. Chem. Phys.* **2014**, 16, 25350- 25357.

24. Yu, B.; Kwak, S. *J. Mater. Chem.* **2012**, 22, 8345-8353.

25. Yu, H.; Zhao, Y.; Zhou, C.; Shang, L.; Peng, Y.; Cao, Y.; Wu, L.; Tung, C.; Zhang, T. *J. Mater. Chem.A* **2014**, 2, 3344-3351.

26. Yu, H.; Shi, R.; Zhao, Y.; Waterhouse, G.; Wu, L.; Tung, C.; Zhang, T. *Adv. Mater.* **2016**, 28, 9454-9477.

27. Gholipour, M.; Dinh, C.; Béland, F.; Do, T. *Nanoscale* **2015**, **7**, 8187-8208.

28. Hou, J.; Cheng, H.; Takeda, O.; Zhu, H. *Energy Environ. Sci.* **2015**, 8, 1348-1357.

29. Lim, S. Y.; Shen, W.; Gao, Z. Q. *Chem. Soc. Rev.* **2015**, 44, 362-381.

30. Zhao, Y. F.; Jia, X. D.; Waterhouse, G. I. N.; Wu, L. Z.; Tung, C. H.; O'Hare, D.; Zhang, T. R. *Adv. Energy Mater*. **2015**, 1501974.

31. Zhang, J. T.; Zhao, Z. H.; Xia, Z.H.; Dai, L. M. *Nature nanotechnology* **2015**, 10, 444-452.

32. Zheng, Y.; Jiao, Y.; Ge, L.; Jaroniec, M.; Qiao, S. Z. *Angew. Chem.* **2013**, 125, 3192-3198.

33. Dua, Y.; Guo, S. J. *Nanoscale* **2016**, 8, 2532- 2543.

34. Duan, J. J.; Chen, S.; Chambers, B. A.; Andersson, G. G.; Qiao, S. Z. *Adv. Mater.* **2015**, 27, 4234-4241

35. Xu, Q.; Liu, Y.; Gao, C.; Wei, J. F.; Zhou, H. J.; Yusheng Chen, Y. S.; Dong, C. B.; Sreeprasad, T. S.; Li, N.; Xia, Z. H. *J. Mater. Chem. C* **2015**, 3, 9885-9893.

36. Sorokin, A. B. *Chem. Rev.* **2013**, 113, 8152-8191.

37. Bottari, G.; Torre, G. D. L.; Guldi, D. M.; and Tomás, T. *Chem. Rev.* **2010**, 110, 6768-6816.

38. Ming, H.; Ma, Z.; Liu, Y.; Pan, K. M.; Yu, H.; Wang, F.; Kang, Z. H. *Dalton Trans.* **2012**, 41, 9526-9531.

39. Moser, F. H.; Thomas, A. L. *J. Chem. Educ.* **1964**, 41, 245-249.

40. Drinkard. W. C.; Bailar, Jr, J. C. *J. Am. Chem. Soc.* **1959**, 81, 4795-4797.

41. Gürek, A. G.; Ahsen, V.; Luneau, D.; Pécaut, J. *Inorg. Chem.* **2001**, 40, 4793-4797.

42. Kirin, I. S.; Moskalev, P. N.; Makashev Russ, Y. A. *J. Inorg. Chem*. **1965**, 10, 1065-1066.

43. Kato, H.; Asakura, K.; Kudo, A. *J. Am. Chem. Soc.* **2003**, 125, 3082-3089.

44. Matsumoto, Y.; Noguchi, M.; Matsunaga, T. *J. Phys. Chem. B* **1999**, 103, 7190- 7194.

45. Abramczyk, H.; Brozek-Pluska, B.; Tondusson, M.; Freysz, E. *J. Phys. Chem. C* **2013**, 117, 4999-5013.

46. Lu, J.; Yang, J. X.; Wang, J. Z.; Lim, A.; Wang, S.; Loh, K. P. *ACS Nano.* **2009**, 3, 2367-2375.

47. Li, X. M.; Zhang, S. L.; Kulinich, S. A.; Liu, Y. L.; Zeng, H. B. *Sci. Rep.* **2014**, 4, 4976-4983.

48. Wang, D. D.; Huang, J.; Li, X.; Yang, P.; Du, Y. K.; Goh, C. M.; Lu, C. *J. Mater. Chem. A* **2015**, 3, 4195-4202.

49. Dou, X. N.; Lin, Z.; Chen, H.; Zheng, Y.Z.; Lu, C.; Lin, J. M. *Chem. Commun.* **2013**, 49, 5871-5873.

50. Ho, W. K.; Zhang, Z. Z.; Lin, W.; Huang, S. P.; Zhang, X. W.; Wang, X. X.; Huang, Y. *ACS Appl. Mater. Interfaces* **2015**, 7, 5497-5505.

51. Liu, R. H.; Huang, H.; Li, H. T.; Liu, Y.; Zhong, J.; Li, Y. Y.; Zhang, S.; Kang, Z. H. *ACS Catal.* **2014**, 4, 328-336.

52. Zhang, C. Z.; Hao, R.; Liao, H. B.; Hou, Y. L. *Nano Energy*. **2013**, 2, 88-97.

53. (a) Zhao, Z. W.; Sun, Y. J.; Luo, Q.; Dong, F.; Hui, L.; Ho, W. K. Less is better. *Sci. Rep.* **2015**, 5, 14643-14657; (b) Milošev, I.; Strehblow, H. H.; Navinšek, B. *Surface and Coatings Technology* **1995**, 74-75, 897-902.

54. Kilian, A. S.; Bernardi, F.; Pancotti, A.; Landers, R.; Siervo, A. D.; Morais, J. *J. Phys. Chem. C* **2014**, 118, 20452-20460.

55. Gu, H. B.; Rapole, S. B.; Huang, Y. D.; Cao, D. M.; Luo, Z. P.; Wei, S. Y.; Guo, Z. H. *J. Mater. Chem. A* **2013**, 1, 2011-2021.

56. Zhang, X.; Hsu, A.; Wang, H.; Song, Y.; Kong, J.; Dresselhaus, M. S.; Tomás, P. *ACS nano*. **2013**, 7, 7262-7270.

57. Du, D. H.; Li, P. C.; Ouyang, J. Y. *ACS Appl. Mater. Interfaces* **2015**, 7, 26952-26958.

58. (a) Lau, V. W.; Mesch, M. B.; Viola Duppel, Volker Blum, Jürgen Senker and Bettina V. Lotsch. *J. Am. Chem. Soc.* **2015**, 137, 1064-1072; (b) Zhang, J.; Wang, Z. J.; Li, L.; Zhao, J. H.; Zheng, J. F.; Cui, H. J.; Zhu, Z. P. *J. Mater. Chem. A* **2014**, 2, 8179-8183.

59. (a) Meng, D. M.; Zhan, W. C.; Guo,Y.; Guo, Y. L.; Wang, L.; Lu, G. Z. *ACS Catal.* **2015**, 5, 5973-5983; (b) Zhang, M. Y.; Shao, C. L.; Guo, Z. C.; Zhang, Jingbo Mu, J. B.; Cao, T. P.; Liu, Y. C. *ACS Appl. Mater. Interfaces* **2011**, 3, 369-377.

60. Guo, M.; Lu, J.Q.; Wu, Y.N.; Wang, Y. J.; Luo, M. F. *Langmuir* **2011**, 27, 3872-3877.

61. Patra, D.; Chiang, C. C.; Chen, W. A.; Wei, K. H.; Wu, M. C.; Chu, C. W. *J. Mater. Chem. A* **2013**, 1, 7767-7774.

62. Xie, G. C.; Zhang, K.; Guo, B. D.; Liu, Q.; Liang, F.; Gong, J. R. *Adv. Mater.* **2013**, 25, 3820-3839.

63. (a) Xie, Y. B.; Yuan, C. W. *Appl. Catal. B: Environ.* **2003**, 46, 251-259; (b) Shi, H. X.; Zhang, T. Y.; An, T. C.; Li, B.; Wang, X. *Journal of Colloid and Interface Science* **2012**, 380, 121-127.

64. Parimi, N. S.; Umasankar, Y.; Atanassov, P.; Ramasamy, R. P. *ACS Catal.* **2012**, 2, 38-44.

65. Liu, X. W.; Zhou, K. B.; Wang, L.; Wang, B.Y.; Li, Y. D. *J. Am. Chem. Soc.* **2009**, 131, 9, 3140-3141.

66. Smrma, D.D.; Hegde, M. S.; Rao, C. N. R. *J. Chem. Soc., Faradsy Trans. 2*, **1981**, 77, 1509-1502.

67. Liu, H.; Feng, Y.; Chen, D.; Li, C. Y.; Lei, C. P.; Yang, J. *J. Mater. Chem. A.* **2015**, 3, 3182-3223.

68. Cao, M. H.; Hu, C. W.; Peng, G.; Qi, Y.J.; Wang, E. B. *J. Am. Chem. Soc.* **2003**, 125, 4982-4983.

69. Li, Q. J.; Liu, B. B.; Wang, L.; Li, D. M.; Liu, R.; Zou, B.; Cui, T.; Zou, G. T. *J. Phys. Chem. Lett.* **2010**, 1, 309-314.

70. Ran, J. G.; Zhang, J.; Yu, J. G.; Jaroniec, M.; Qiao, S. Z. *Chem. Soc. Rev.* **2014**, 43, 7787-7812.

Table of Contents graphic